CrossMark

ORIGINAL PAPER

Numerical Approach for Goaf-Side Entry Layout and Yield Pillar Design in Fractured Ground Conditions

Lishuai Jiang[1,2,3] · Peipeng Zhang[1] · Lianjun Chen[1] · Zhen Hao[4,5] ·
Atsushi Sainoki[6] · Hani S. Mitri[2,7] · Qingbiao Wang[1]

Abstract Entry driven along goaf-side (EDG), which is the development of an entry of the next longwall panel along the goaf-side and the isolation of the entry from the goaf with a small-width yield pillar, has been widely employed in China over the past several decades . The width of such a yield pillar has a crucial effect on EDG layout in terms of the ground control, isolation effect and resource recovery rate. Based on a case study, this paper presents an approach for evaluating, designing and optimizing EDG and yield pillar by considering the results from numerical simulations and field practice. To rigorously analyze the ground stability, the numerical study begins with the simulation of goaf-side stress and ground conditions. Four global models with identical conditions, except for the width of the yield pillar, are built, and the effect of pillar width on ground stability is investigated by comparing aspects of stress distribution, failure propagation, and displacement evolution during the entire service life of the entry. Based on simulation results, the isolation effect of the pillar acquired from field practice is also considered. The suggested optimal yield pillar design is validated using a field test in the same mine. Thus, the presented numerical approach provides references and can be utilized for the evaluation, design and optimization of EDG and yield pillars under similar geological and geotechnical circumstances.

✉ Lishuai Jiang
lsjiang@sdust.edu.cn

✉ Lianjun Chen
creejxk@163.com

1 State Key Laboratory of Mining Disaster Prevention and Control, Shandong University of Science and Technology, Qingdao 266590, China

2 Department of Mining and Materials Engineering, McGill University, Montreal H3A 2A7, Canada

3 State Key Laboratory for GeoMechanics and Deep Underground Engineering, China University of Mining and Technology, Beijing 100083, China

4 Faculty of Resources and Safety Engineering, China University of Mining and Technology, Beijing 100083, China

5 Zhaogu No.2 Coal Mine, Henan Energy and Chemical Industry Group Co., Ltd., Xinxiang 453633, China

6 International Research Organization for Advanced Science and Technology, Kumamoto University, Kumamoto 860-8555, Japan

7 School of Civil Engineering, Henan Polytechnic University, Jiaozuo 454000, China

1 Introduction

The stability of roadways is a long-standing issue in underground coal mines, especially for entries that serve and ensure the safe production of longwall panels. The ground stability and failure mechanisms of entries vary depending on stress, geological and geotechnical conditions.

Entry driven along goaf-side (EDG), which is the development of an entry of the next longwall panel along the goaf-side and the isolation of the entry from the goaf with a small-width yield pillar, has been widely employed in China over the past several decades (Li et al. 2015; Wang et al. 2015; Tan et al. 2015; Zhang et al. 2017). A yield pillar, which is designed to deform progressively during its service life, can transfer its load to adjacent abutments and control the mining-induced stress

distribution around the entries (Peng 2008). Hence, it contributes to preventing coal bumps and excessive ground deformation by employing yield pillars, and it has been successfully applied in many coal mines of China and USA (Peng 2008; Li et al. 2015; Chen et al. 2016). For instance, Carr et al. (1985) employed a yield-abutment-yield pillar layout to a four-entry longwall system in the Blue Creek seam in Alabama to control its severe floor deformation. The application of yield pillars in Utah coal fields has achieved a notable effect on preventing coal bumps (Peperakis 1958; Agapito et al. 1988).

The width of a yield pillar is a crucial factor in EDG layout. Its effect and importance are based on three aspects. First, the stress environment before entry excavation varies with pillar width. By employing a small-width yield pillar, the mining-induced stress concentrated area can be avoided, which contributes to stability control (e.g., ground deformation, coal bump potential). Second, the yield pillar plays an important role in isolating water, gas and caved rock from the adjacent goaf. Thus, the isolation effect generally presents a positive correlation with pillar width. In addition, the resource recovery rate of the seam is directly influenced by the pillar width, especially for longwall panels that have over thousand meters of strike length.

Yield pillar design can be divided into three types (Peng): trial-and-error, empirical and analytical methods.

The trial-and-error method needs continuous field applications for a long period of time. A well-known empirical method for yield pillar design is converging pillar experiments (Serata 1982; Carr et al. 1984, 1985), which use tapering pillars to produce continuous variation of the yield pillar width. Using analytical methods, considerable research has been carried out (Tsang and Peng 1993; Morsy 2003). For instance, Wilson (1982) adapted his pillar design concept to American longwall multiple entry systems by combing both yield and abutment pillars in an integrated manner. Chen (1989) considered the yield pillar to be a pillar without an elastic core and proposed expressions of three types of yield pillar widths by combing numerical modeling and Wilson's confined core concept. This method was developed by introducing three criteria in 1999 (Chen and Peng 1999).

In recent years, an increasing number of yield pillar width studies have been performed with numerical modeling methods. Li et al. (2015) studied the effect of yield pillar's width/height ratio on stress distribution based on an EDG case study in China. Their results indicated that the ratio of vertical stresses in the two ribs can be used for the yield pillar design. New approaches for yield pillar design were studied based on geological conditions of a highly gassy coal mine in China (Yan et al. 2013; Zhang et al. 2015). Wang et al. (2015) studied the failure mechanism of a deep goaf-side entry and its control strategies.

In the present study, a comprehensive numerical method for yield pillar design and optimization has been proposed based on a case study conducted in the Zhaogu No.2 coal mine. In this numerical method, multiple factors that accord with field practice have been considered, including the extent of disturbed zones, caved rock compaction simulation, and fracture-induced ground weakening. The numerical approach considers simulation results (stress distribution, failure extent and ground displacement), field feedback (gas concentration, water inflow) and resource recovery rate, and the design and optimization of the yield pillar are comprehensively investigated.

2 Case Study

2.1 Geological and Geotechnical Overview of the Zhaogu No.2 Mine

The Zhaogu No.2 mine is located in Xinxiang City, Henan Province, China. A retreating-longwall method is employed to all panels. The coal seam is nearly horizontal and has a mean thickness of 6.12 m.

This case study site is situated at the headentry of panel 11,030 at a depth of approximately 625 m. The panel is approximately 180 m wide along its dip and 2000 m long along its strike. This panel is extracted with a large-height full-seam mining method, which means that the coal seam within the panel region will be extracted in one retreat. The target roadway, the headentry of panel 11,030, is the first EDG in the mine and considered a field trial for studying the feasibility and applicability of the goaf-side entry layout in the Zhaogu No.2 coal mine. The entry is driven along the goaf of 11,010 with an 8-m-wide yield pillar, as illustrated in Fig. 1.

According to the study that was conducted at the same mine (Jiang et al. 2016), a typical geological column based on core logging was carried out in an adjacent panel 11,050, as shown in Fig. 2. The roof strata of this panel are mainly composed of mudstone, sandy mudstone and sandstone.

The dimension of the target entry is 3.3 m in height and 4.8 m in width. The gateroad is driven along the roof line of the thick coal seam, which leads to the ribs and immediate floor consisting of coal. Rebar bolts, cable bolts and hydraulic pillars are employed as the primary support, and wire mesh is utilized to prevent rock falling, as shown in Fig. 3. Rebar bolts are installed both in the roof and ribs on a square pattern of 800 mm × 800 mm. Cable bolts are installed in the roof with an 800 mm spacing and 1300 mm between rows. Both Rebar and Cable bolts are partially grouted with resin cartridges, and the relevant mechanical parameters are shown in Table 1. Hydraulic pillars (model: DW35-200/100), whose setting load is 100 kN and
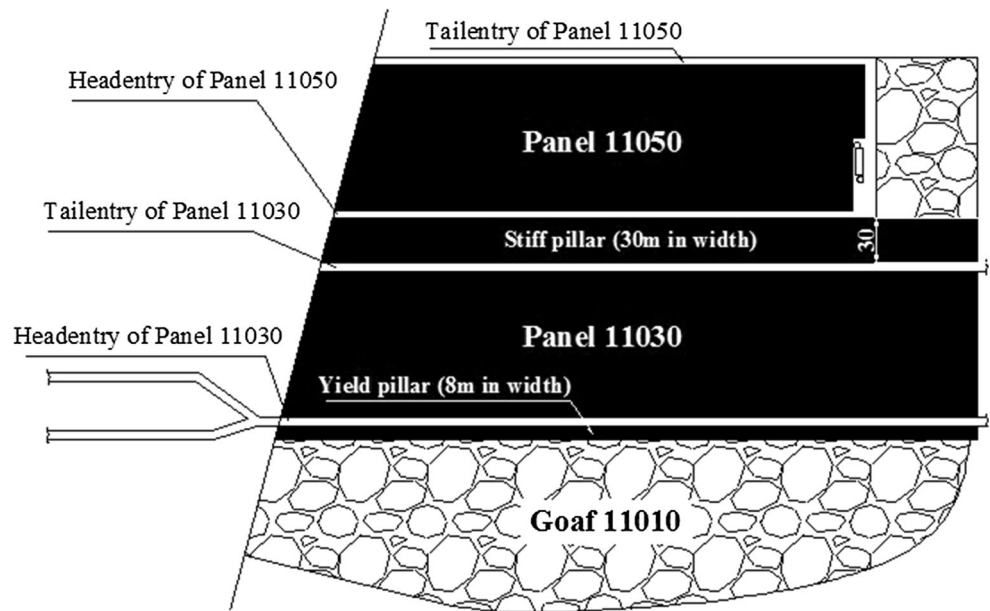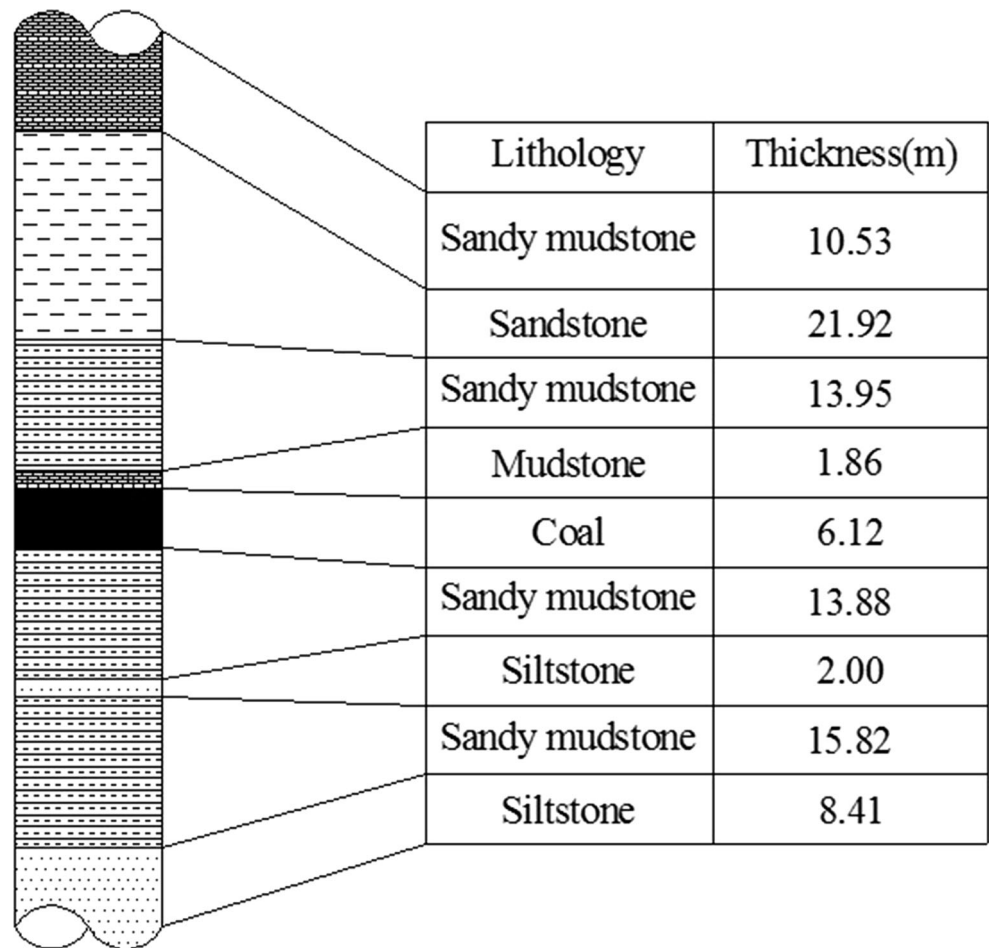
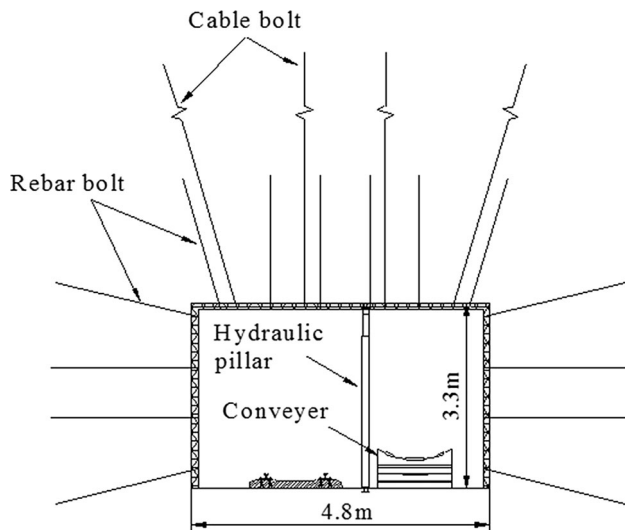**Fig. 1** Plan view of local panel layout

Fig. 2 Typical geological column

Lithology	Thickness(m)
Sandy mudstone	10.53
Sandstone	21.92
Sandy mudstone	13.95
Mudstone	1.86
Coal	6.12
Sandy mudstone	13.88
Siltstone	2.00
Sandy mudstone	15.82
Siltstone	8.41

Fig. 3 Entry support design

Table 1 Mechanical parameters of Rebar and cable bolt

Type	L (mm)	L_r (mm)	D (mm)	F_t (KN)
Rebar bolt	2400	1200	20	225
Cable bolt	8250	2400	21.6	510

L is length of support element, L_r is resin grout length, D is diameter, F_t is tensile strength

maximum height is 3500 mm, are installed every 1000 mm between rows.

2.2 Rock Mechanical Properties Experiment

Laboratory experiments were conducted on collected rock core samples, as shown in Fig. 4. The experiments were carried out using a servo-controlled testing system (RMT-150B). The failure duration curves of the samples exhibit a significant brittle behavior. The experimental results are listed in Table 2 (after Jiang et al. 2016). Note that average values are shown in the table.

2.3 Field Monitoring and Observation

As stated in *Introduction*, an application evaluation of the goaf-side entry layout includes ground stability and should consider the gas emission rate, water inflow, coal and gas burst potential, and resource recovery rate. Therefore, comprehensive field monitoring and observation, including ground deformation, gas emission, water inflow and other safety issues, are essential to assess the trial layout of the headentry.

The photographs of field observations during the entry development period are shown in Fig. 5. As seen, even without the influence of mining activities, the surrounding rocks of this entry are already excessively deformed, which is

accompanied by severe fracturing. A sketch of ground deformation is illustrated in Fig. 5a and shows a notable asymmetric deformation pattern. The roof and rib on the left side of the pillar (left side of Fig. 5a) have worse stability than that observed on the right side of the pillar (solid coal). As shown in Fig. 5b, at some locations along the entry, hydraulic pillars are over-compressed by the roof-floor convergence, and I-beams that connect cable bolts bend due to the roof sag. The surrounding rocks are fractured into small and loose fragments. This leads to rock fall (roof caving and rib spalling). The severe deformation may reduce the functionality of the entry by damaging the rail and conveyer.

To provide sufficient data to examine the deformation characteristics and ground control, a deformation-monitoring program, which includes 42 monitoring stations set up within a length of 702 m, from T110 to T812 (distance to entrance of the entry), of the entry is illustrated in Fig. 1. The deformation data from four monitoring stations that are uniformly distributed in the monitoring segment are shown in Fig. 6. For clarification, "#11-T255" in Fig. 6a denotes the No. 11 station of the total 42 monitoring stations that are located at 255 m from the entrance of the entry. The monitoring stations are set right after excavation, which leads to the difference in monitoring data, and the data are dependent on the stress readjustment due to entry development. The missing data within the monitoring period are caused by monitoring points being obstructed due to equipment or materials. It can be seen that the roof sag is markedly smaller than are the floor heave and rib convergence. The average displacements of monitoring stations are 134.3, 402.2, 585.6 mm for the roof sag, floor heave and rib convergence, respectively. To prevent the excessive floor heave from influencing the functionality of rail and conveyer, floor shoveling is needed in some locations, which results in a sudden drop in some of the deformation curves. It is expected that the primary cause of such characteristics of ground deformation is the geological properties of the surrounding rock. Since the entry is driven along the roof line of a thick coal seam, the immediate floor and two ribs are composed of coal, and the immediate roof is composed of mudstone. The weak properties of coal make the floor and two ribs less stable, thereby causing large deformations. In addition, a significant creep behavior can be observed, and it is one of the major stability characteristics of EDG according to previous studies (Hou 2013). The average deformation rates of floor heave and ribs convergence reach 6.5 and 8.7 mm/d, respectively.

Authenticated by the Research Center of Coal Mine Safety Engineering and Technology, Henan Polytechnic University, the Zhaogu No.2 coal mine has a potential for coal and gas burst, but it is a non-burst area above the 850 m level. For safety concerns, the monitoring of gas emission is conducted during the panel service life, and the warning value of gas concentration is set to 0.7%. During

Fig. 4 Rock core samples for the mechanical properties experiment. **a** Core samples obtained from the field, **b** rock specimens after processing, **c** failure pattern
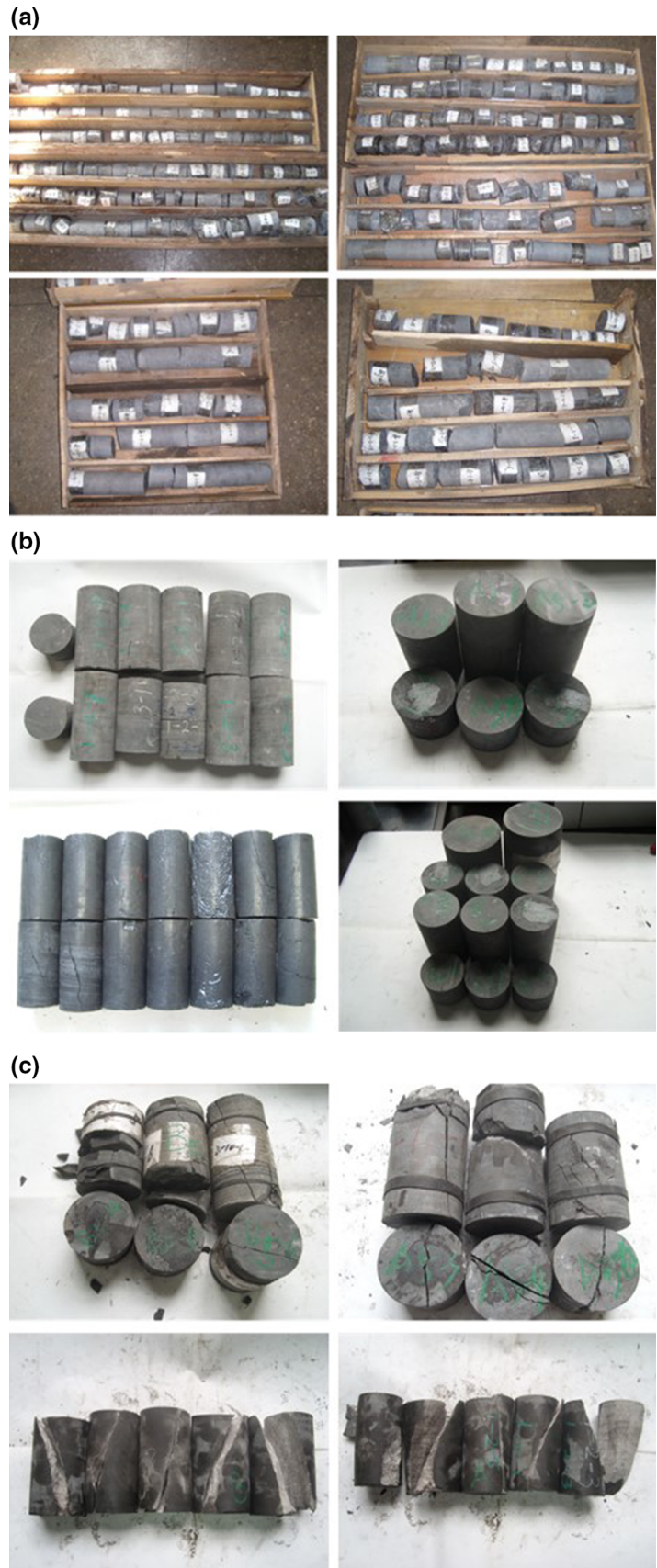
(a)

(b)

(c)

Table 2 Rock mechanical property test results

Strata	Lithology	σ_t (MPa)	σ_c (MPa)	E_i (GPa)	υ
Roof	Sandstone	10.91	83.6	31.6	0.23
	Sandy mudstone	3.47	56.2	16.3	0.25
	Mudstone	2.34	38.2	9.5	0.29
Coal seam	Coal	0.72	20.4	2.8	0.30
Floor	Sandy mudstone	2.81	41.8	9.9	0.27
	Siltstone	13.52	99.6	82.6	0.22

σ_t is tensile strength, σ_c is uniaxial compressive strength, E is modulus of elasticity, υ is Poisson's ratio
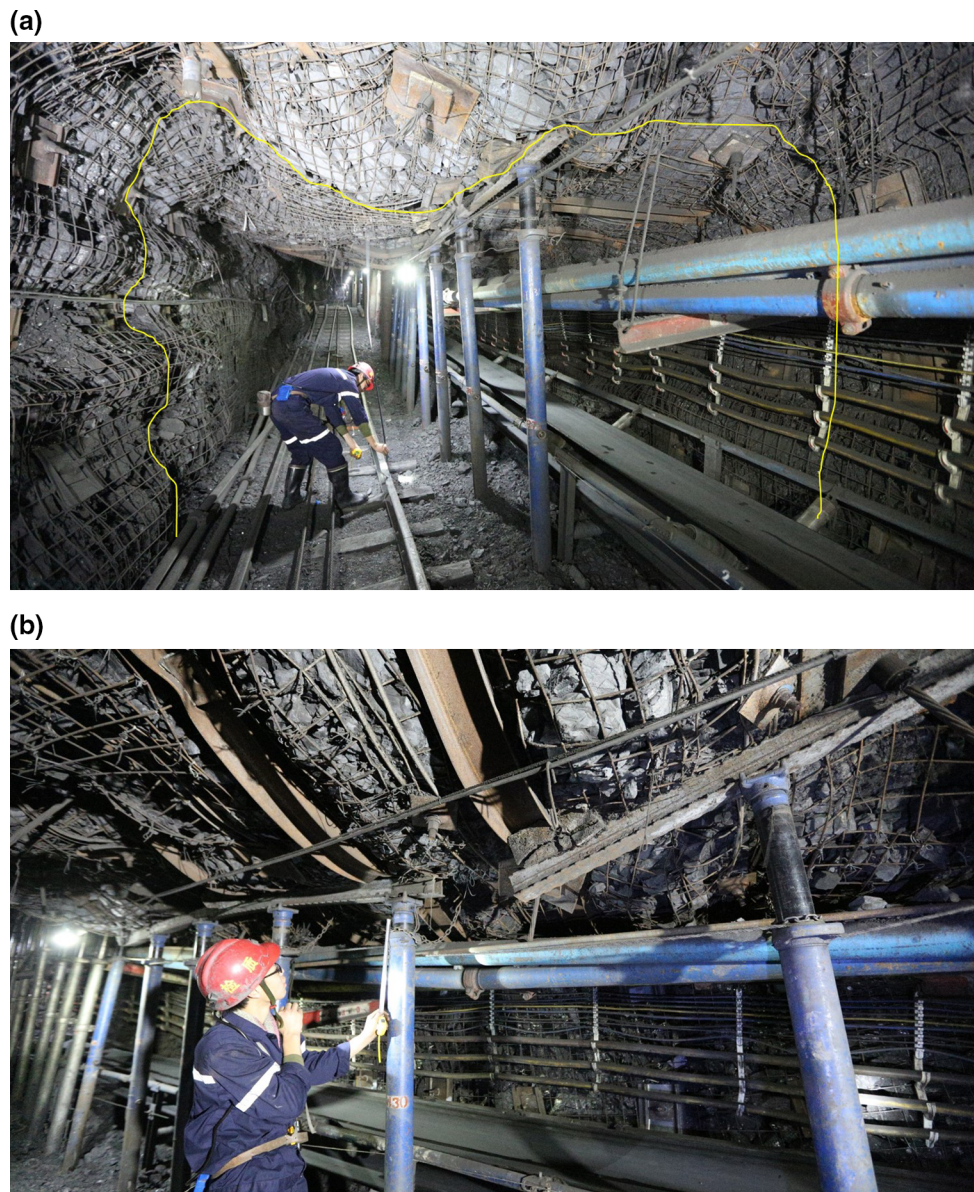
(a)

(b)

Fig. 5 Field monitoring and observation of ground stability. **a** Sketch of the deformation pattern and **b** over-compressed hydraulic pillar

the service life of panel 11,030, the maximum gas emission rate and concentration are 0.6 m³/min and 0.3%, respectively. In addition, according to field monitoring, no incident and sign of water inflow occurred. Thus, the yield pillar with a width of 8 m played an important role in gas and water isolation.

2.4 Summary of the case study

Using the rock properties experiments, field observation and monitoring, the ground conditions (including rock failure, deformation, gas emission and water inflow) of the trial EDG layout have been comprehensively investigated. By employing an 8-m-wide yield pillar, the headentry of panel 11,030 shows good control for safety issues of gas or water. However, excessive deformation and poor stability have become the primary issues, and severe fractures and large deformations can significantly destabilize the surrounding rock, which leads to potential safety issues and economic losses due to gateroad repair and secondary support installation. The aforementioned field feedback of the trial EDG practice requires further investigation and optimization of the EDG layout or yield pillar design. In the following sections, a numerical analysis of the case study is conducted using the three-dimensional finite-difference software FLAC3D.

3 Numerical Analysis of the Goaf-Side Stress and Ground Condition

Since EDG is excavated right next to a mined goaf, its stress and ground conditions differ markedly from those of an entry that is excavated in solid rock. Hence, a simulation of mining and induced stress readjustment and strata movement of the last goaf is a prerequisite for EDG simulation.

3.1 Extent of Disturbed Zones Due to Mining

After coal is extracted step by step, a void (goaf) behind the face is created, caved rocks fall from the roof and fill the goaf, and the caved loose rock will be compacted more stiffly and densely due to the compression of the overlying strata. Responding to longwall mining activities, the overlying strata can be classified into three disturbed zones, depending on their structural characteristics (Peng 2008), as illustrated in Fig. 7. The extent of each zone depends on the mining height, geological circumstances, and rock mass properties of the overlying strata. Based on an abundance of field data obtained in Chinese coalfields, the following expressions proposed by Bai et al. (1995) are employed to estimate the extent of caved and fractured zones:

$$\begin{cases} H_c = \dfrac{100h}{c_1 h + c_2} \\ H_f = \dfrac{100h}{c_3 h + c_4} \end{cases} \tag{1}$$

where H_c is the height of the caved zone, H_f is the height of the fractured zone, h is the mining height, and $c_1 \sim c_4$ are
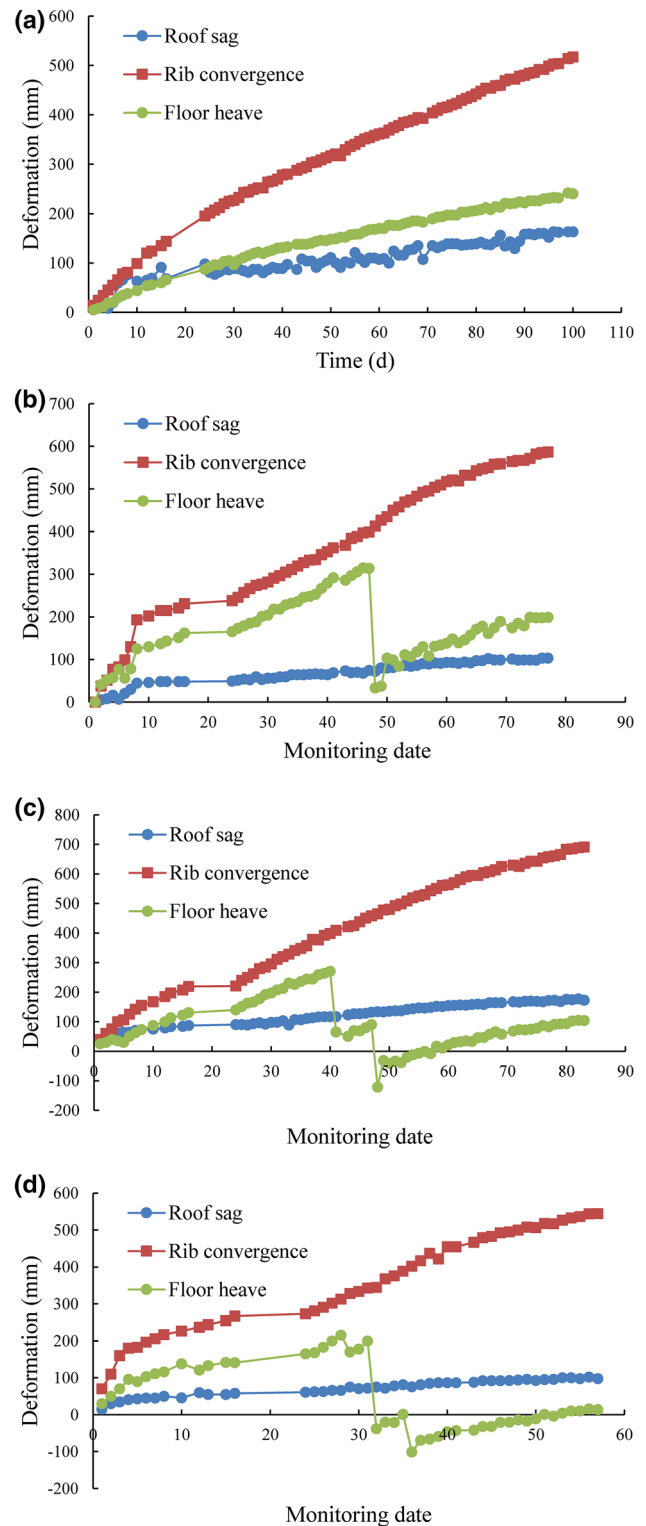

Fig. 6 Field deformation monitoring of the four stations. a #11-T255, b #24-T529, c #35-T734, d #41-T802

the coefficients that depend on strata lithology (Table 3). According to the rock properties experiment presented in Sect. 2.2 and the large-height mining practice of panel

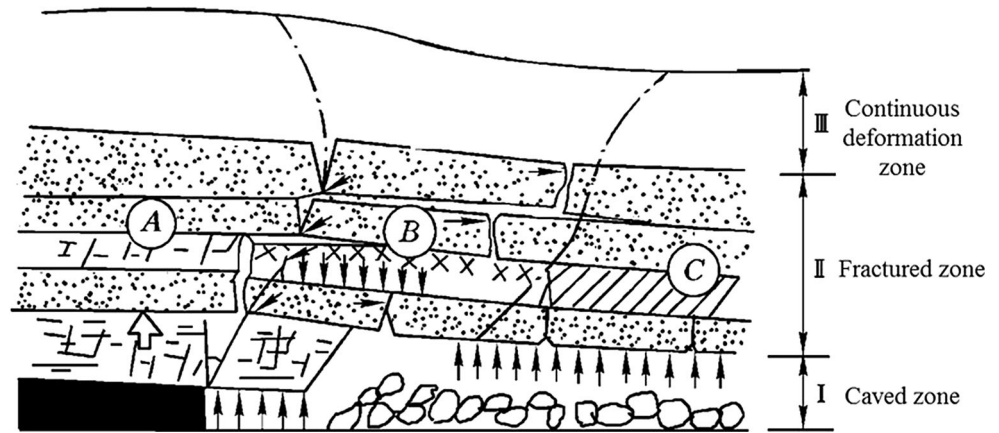**Fig. 7** Disturbed zones due to longwall mining (after Peng 2008)

Table 3 Coefficients for height of caved and fractured zones (Bai et al. 1995)

Strata lithology	Compressive strength, σ_c (MPa)	C_1	C_2	C_3	C_4
Strong and hard	>40	2.1	16	1.2	2
Medium strong	20–40	4.7	19	1.6	3.6
Soft and weak	<20	6.2	32	3.1	5

11,030, the heights of caved and fractured zones of panel 11,030 are estimated to be 12.7 and 45.5 m, respectively.

3.2 Simulation of goaf-side stress and ground condition

The mechanical behavior of caved rock during compaction is essential in numerical simulation of the aforementioned process. A stress–strain relationship of the goaf material proposed by Salamon (1990) is widely accepted and was applied in previous studies on longwall coal mining (Yavuz 2004; Li et al. 2015; Zhang et al. 2015):

$$\sigma = \frac{E_0 \varepsilon}{1 - \varepsilon/\varepsilon_m} \tag{2}$$

where σ is the uniaxial stress applied to the material, ε is the strain occurring under the applied stress, E_0 is the initial tangent modulus, and ε_m is the maximum possible strain of the bulked rock material. E_0 largely depends on the bulking factor b and strength of rock pieces σ_c. An expression obtained from a three-dimensional regression analysis by Yavuz (2004) gives the relationship between these parameters as follows:

$$E_0 = \frac{10.39 \sigma_c^{1.042}}{b^{7.7}} \tag{3}$$

ε_m can be determined as

$$\varepsilon_m = \frac{b-1}{b} \tag{4}$$

By substituting Eqs. (3) and (4) into (2), the stress–strain relationship of the goaf material can be expressed as

$$\sigma = \frac{10.39 \sigma_c^{1.042}}{b^{7.7}} \cdot \frac{\varepsilon}{1 - \frac{b}{b-1} \varepsilon} \tag{5}$$

3.3 Back Analysis for the Goaf Compaction Simulation

The double-yield model embedded in FLAC3D is a well-accepted approach for simulating the mechanical behavior of goaf under compaction (Yavuz 2004; Li et al. 2015; Zhang et al. 2015). Using laboratory tests, the bulking factor b of the coal seam is estimated to be 1.47, and the maximum possible strain is determined to be 0.32 by substituting $b = 1.47$ into Eq. (4). Hence, the stress–strain relationship of goaf 11,030, i.e., the input table of cap pressure of the double-yield model, can be obtained by substituting the aforementioned parameters into Eq. (5).

In addition to cap pressure, other input rock mass properties of the double-yield model must be obtained via back analysis. A cube sub-model is built, and its loading is simulated by applying a vertical velocity at the top boundary while the side boundaries are confined. Using trial-and-error modeling, the double-yield model, whose mechanical behavior shows good agreement with Salamon's expression (illustrated in Fig. 8), has been acquired, and the input properties are listed in Table 4.

3.4 Numerical Model of the Fractured Ground Condition

For a realistic simulation of the fractured ground condition, an innovative modeling technique, the tension-weakening model, is employed. The tension-weakening model, which is developed and implemented into FLAC3D by Jiang et al. (2016), is suitable for numerical simulation under the fractured condition by considering the fracturing intensity and its weakening effect on rock mass. The tension-weakening model is developed based on the strain-softening model, which employs the Mohr–Coulomb failure criterion as

$$\sigma_1 - \frac{2c(\{\varepsilon^{\mathrm{mp}}\})\cos\phi(\{\varepsilon^{\mathrm{mp}}\})}{1-\sin\phi(\{\varepsilon^{\mathrm{mp}}\})} - \frac{1+\sin\phi(\{\varepsilon^{\mathrm{mp}}\})}{1-\sin\phi(\{\varepsilon^{\mathrm{mp}}\})}\sigma_3 = 0 \tag{6}$$

where $\varepsilon^{\mathrm{mp}}$ is the maximum principal plastic strain. After shear failure occurs, the strength parameters decrease with plastic strain. If the tension failure occurs, Young's modulus is decreased to a residual value to represent the tension-induced fracturing equivalently. The tension-weakening model can progressively examine the failure state of each zone in the model and weaken its properties accordingly. This overcomes the limitation of conventional simulation techniques. Specifically, elastic modulus is kept constant, regardless of the rock mass failure and fracture propagation. A novel indicator, GSI_t, is defined as the intensity of tensile fractures to describe E_r, the residual elastic modulus of rock mass after tensile failure occurs, with the following equation:

$$E_r = \sqrt{\frac{\sigma_{\mathrm{m}}}{100}} \cdot 10^{\left(\frac{GSI_t - 10}{40}\right)} \tag{7}$$

According to the field investigation of this case study, GSI_t is estimated as 50 for the numerical analysis. By employing the tension-weakening model, the fracturing-induced rock mass weakening due to mining is simulated, which provides a more rigorous way for simulating rock mass behavior under such conditions compared with the perfect elasto-plastic and strain-softening models.

3.5 Verification of Simulation of Goaf-Side Stress Environment

Verifying the simulated goaf-side stress environment, incorporating the verification of goaf material, tension-weakening model and weakening parameter, and simulated mining process, is essential for the subsequent EDG stability simulation. Considering the symmetry of the panel with respect to its centerline, a local numerical model of panel 11,010 is generated, as shown in Fig. 9. According to
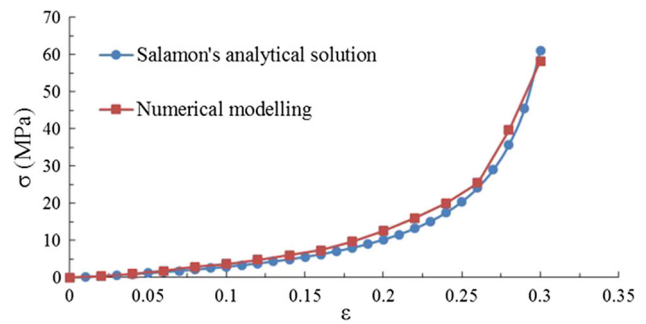

Fig. 8 Comparison of the stress–strain relationship between Salamon's model and the numerical model

Table 4 Properties of double-yield model

K (MPa)	G (MPa)	γ (Kg/m^{-3})	C (MPa)	φ (°)	σ_t (MPa)
19900	1000	1700	0.001	30	0

the surrounding strata illustrated in Fig. 2, the dimensions of this local model are 180 m in width, 350 m in length and 100 m in height, which are determined based on model sensitivity analysis of model size and mesh density. A gravity force of 9.8 N/kg is applied to the entire model, and a vertical load of 15 MPa is applied to the top model boundary, simulating overburden pressure by assuming that the overlying unit weight is 0.025 MN/m^3. The model lateral boundaries allow no displacement to occur in the direction perpendicular to the boundaries. In situ stresses are applied according to a study carried out in the same mine (Jiang et al. 2016). The rock mass properties for simulation, as listed in Table 5, are estimated from the intact rock properties (Table 2) and using the generalized Hoek–Brown failure criterion (Hoek et al. 2002). The simulation process of retreat mining is as follows: (i) apply in situ stress state, (ii) extract the coal seam in retreat by 10 m along the mining direction for each cycle, (iii) fill caved zone with double-yield model, and (iv) repeat (ii) and (iii) after the calculation reaches equilibrium until the entire panel is mined out.

As shown in Fig. 10, after panel 11,010 is mined out, the front and side abutment pressure over coal seam and stress recovery in goaf due to compaction can be observed. A monitoring line for the abutment pressure over side coal seam, where headentry and panel 11,030 are planned, is marked with a dotted line. As seen, the vertical stress varies along the y-direction (strike direction of panel) due to the location of the working face. Unlike the unstable strata and stress circumstance near the face, the surrounding strata far behind the face have basically stabilized after stress readjustment and strata movement. Thus, their stress distribution provides a better reference for verification.

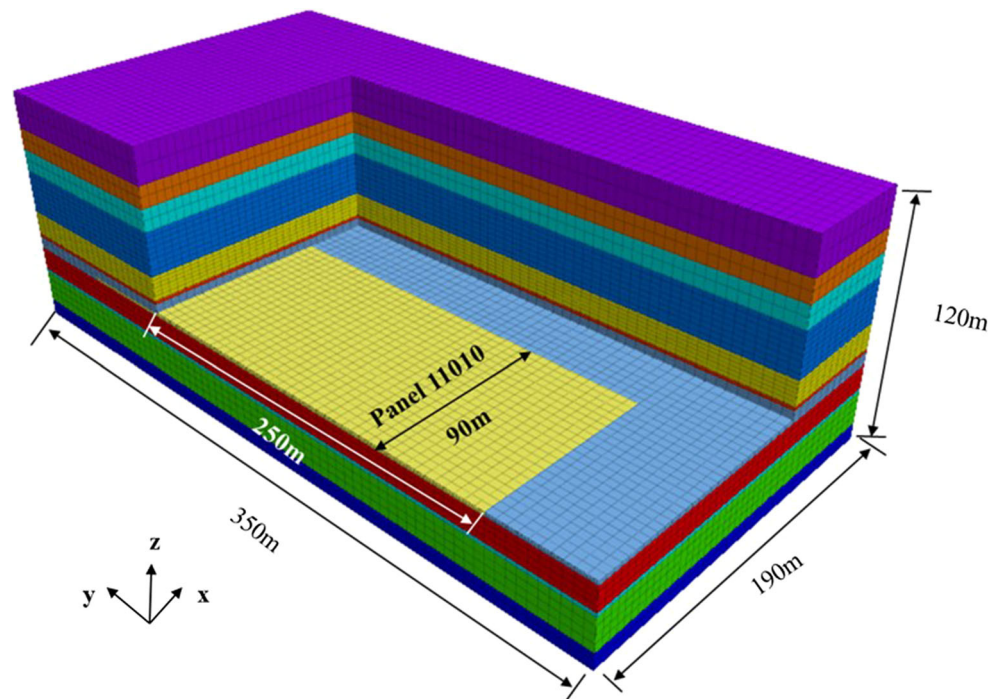**Fig. 9** Local model for verifying the goaf-side stress environment

Table 5 Rock mass mechanical properties

Strata	Lithology	K (GPa)	G (GPa)	C (MPa)	σ_t (MPa)	φ (deg.)	C_r (MPa)	ε_p (%)
Roof	Sandstone	9.1	5.9	3.9	2.3	45	0.39	0.01
	Sandy mudstone	5.2	3.1	3.2	1.8	40	0.32	0.01
	Mudstone	2.4	1.1	2.1	0.8	35	0.21	0.01
Coal seam	Coal	1.3	0.6	1.4	0.3	31	0.14	0.01
Floor	Sandy mudstone	7.2	4.0	3.4	2.2	37	0.34	0.01
	Siltstone	9.6	6.5	4.2	3.5	47	0.42	0.01

K is bulk modulus, G is shear modulus, c is cohesion, σ_t is tensile strength, φ is friction angle, c_r is residual cohesion, ε_p is plastic strain parameter at the residual strength

4 Numerical Analysis of Ground Stability of EDG

The ground and stress environment of EDG are formed after strata movement and stress readjustment, which are induced by the mining activities of an adjacent panel. As illustrated in Fig. 10, with an increase in the planned yield pillar width, the initial stress state increases significantly before the EDG excavation. The high stress release due to excavation may lead to pronounced ground convergence and rock burst potential (Zhao et al. 2017). Meanwhile, the low-stress zone in the pillar is caused by the distress-yielding or failure of rock mass due to the influence of adjacent mining. With a decrease in pillar width, a worse ground condition prior to excavation is expected. Thus, rock mass will be more susceptible to excavation-induced stress redistribution, which may further result in rock mass being prone to deform and fail, or non-ideal support performance due to loose rock.

Therefore, studies on yield pillar design or location optimization of EDG should be based not on a single-factor analysis but on a comprehensive research over multiple factors. In the presented numerical study, the effect of pillar width on ground stability has been investigated in terms of stress distribution, failure propagation, and displacement evolution in periods of both entry development and retreat mining. The results support the yield pillar design studies.

4.1 Model Description

Based on a previous study, a global model, which encompasses panels 11,010 and 11,030, headentry of panel 11,030 and the case yield pillar (8 m in width), is generated for the stability analysis of the headentry, as shown in Fig. 11a. In addition, three global models that differ from the case study in only their yield pillar widths (3, 5 and
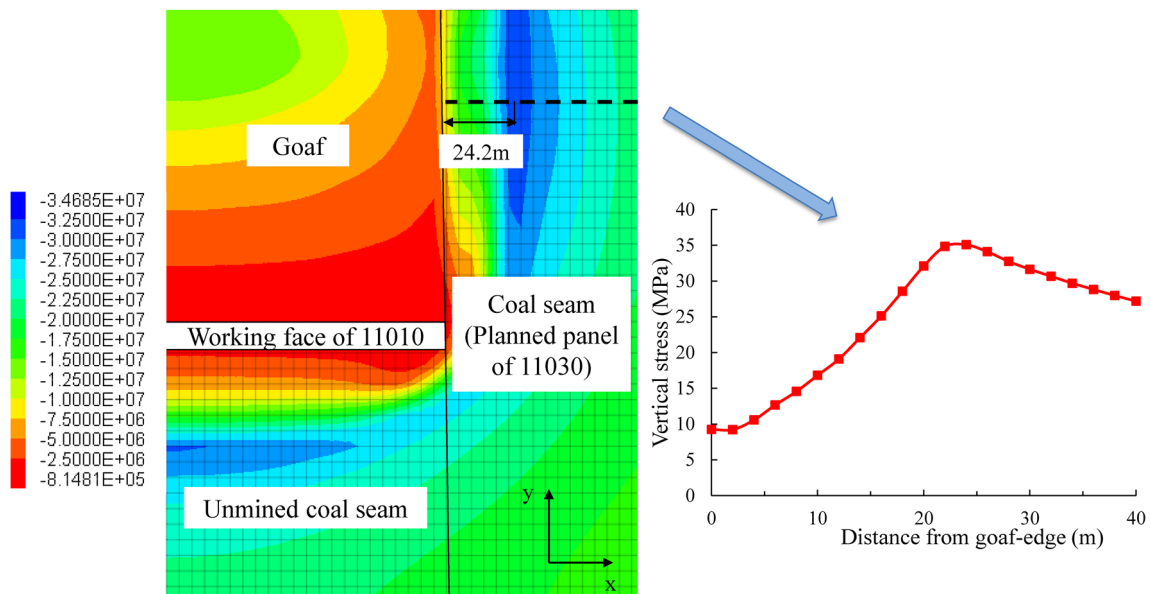
Fig. 10 Monitoring line and curve mining-induced abutment pressure over a side coal seam

11 m) are built to study the effect that pillar width has on EDG stability. By employing the symmetric principle, the half widths of the two panels are simulated. Otherwise, the model is be too large for stability analysis of the entry in the middle. The global model, which is built according to the field practice, is denoted as Model-8 m (8 m stands for the width of the yield pillar), and the other three models are similarly denoted as Model-3 m, Model-5 m and Model-11 m.

Based on the same field situation, these four global models are identical to the local model (e.g., strata layout, constitutive model, rock mass properties, boundary conditions) presented in Fig. 9, except for the yield pillar width and model dimension in the x-direction.

After panel 11,010 is mined out using the simulation process introduced in Sect. 3.5, the EDG stability analysis is performed as follows: (i) excavate the headentry of panel 11,030 by 10 m along the strike, (ii) apply the primary support right after the excavation, (iii) repeat (i) and (ii) after the calculation reaches equilibrium until the development of the entry is complete, (iv) extract panel 11,030 during a 10-m retreat along the mining direction for each cycle, (v) fill the caved zone with the double-yield model, and (vi) repeat (iv) and (v) after the calculation reaches equilibrium until the entire panel is mined out. One monitoring station is set up, as shown in Fig. 11a. The ground failure and deformation are monitored to investigate the EDG stability both during the entry development and retreat mining periods. As shown in Fig. 11b, the support design of this entry is simulated with structural elements, which are embedded in FLAC3D and can be utilized to simulate various rock supports. Since Rebar and Cable

bolts, hydraulic pillars and steel beams are employed as the primary support in practice, two different types of structural elements (cable and beam) are utilized for the support simulation. The properties of structural elements follow the relevant support mechanical parameters presented in Sect. 2.1.

4.2 Stress Distribution

The vertical stress distribution at the monitoring station after EDG development with a different yield pillar width is shown in Fig. 12. Note that $\sigma_{z\text{-pillar}}$ and $\sigma_{z\text{-seam}}$ refer to the maximum vertical stress in yield pillar and coal seam, respectively, and their locations can be observed from contours.

As seen, both $\sigma_{z\text{-pillar}}$ and $\sigma_{z\text{-seam}}$ show positive correlations with pillar width, which agrees with the distribution characteristics before excavating the headentry (Fig. 10). Within the ultimate equilibrium zone, the initial stress increases with an increase in pillar width, as do $\sigma_{z\text{-pillar}}$ and $\sigma_{z\text{-seam}}$ after EDG development. The considerable stress difference results in a different degree of burst potential, for which the models with smaller pillars exhibit benefits in burst prevention. The increase in pillar width leads to a notable increase in $\sigma_{z\text{-seam}}$ but barely affects the distance between the location of $\sigma_{z\text{-seam}}$ and entry surface.

4.3 Extent of Ground Failure

The extent and state of failure zones are key parameters for entry stability analysis, and support design. However, unlike an entry driven in solid rock, the failure zones of
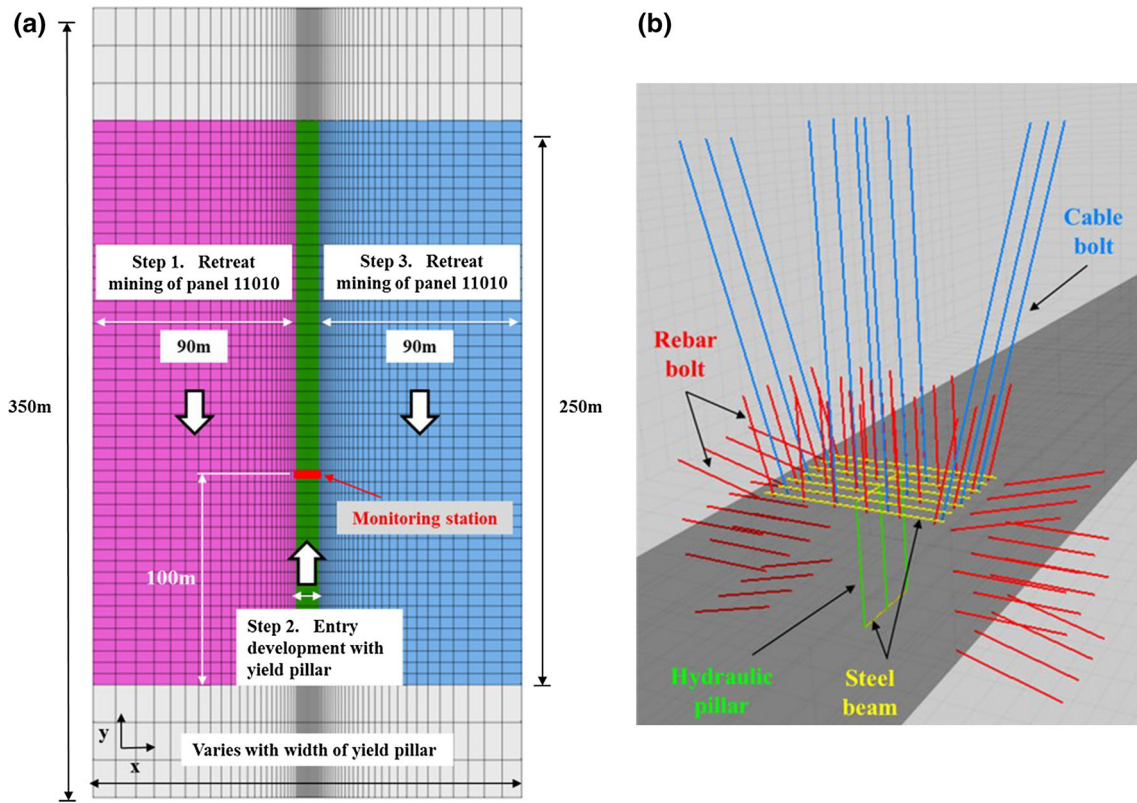
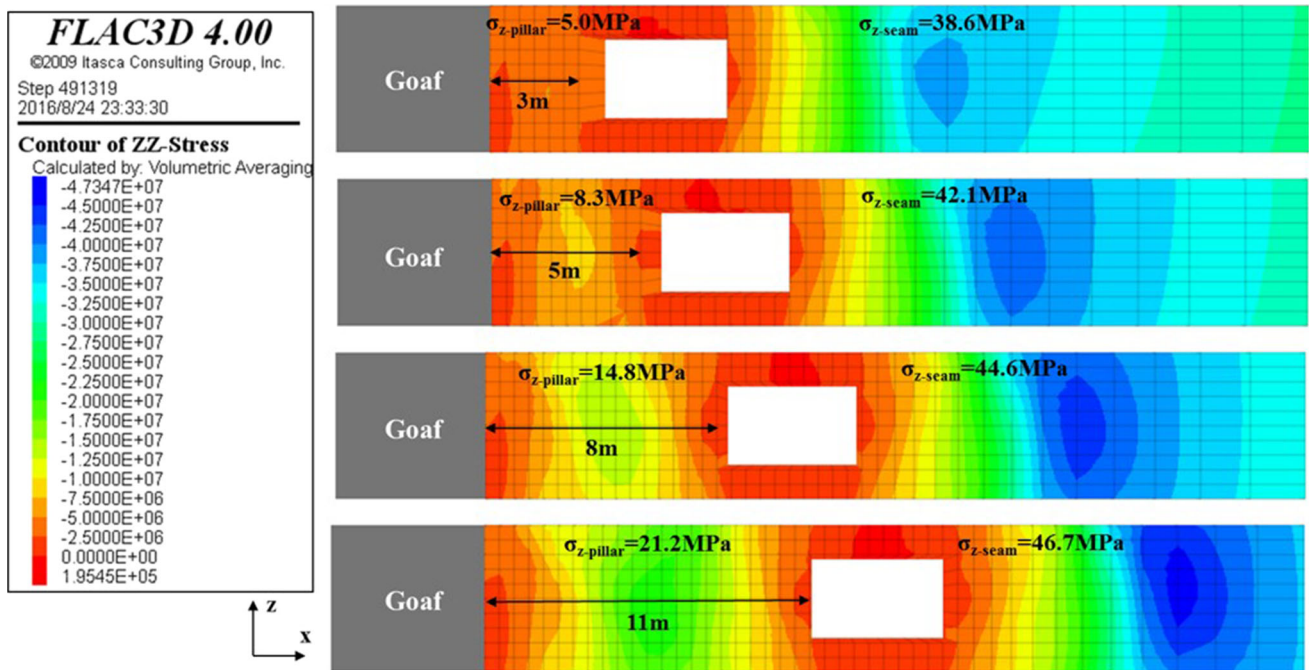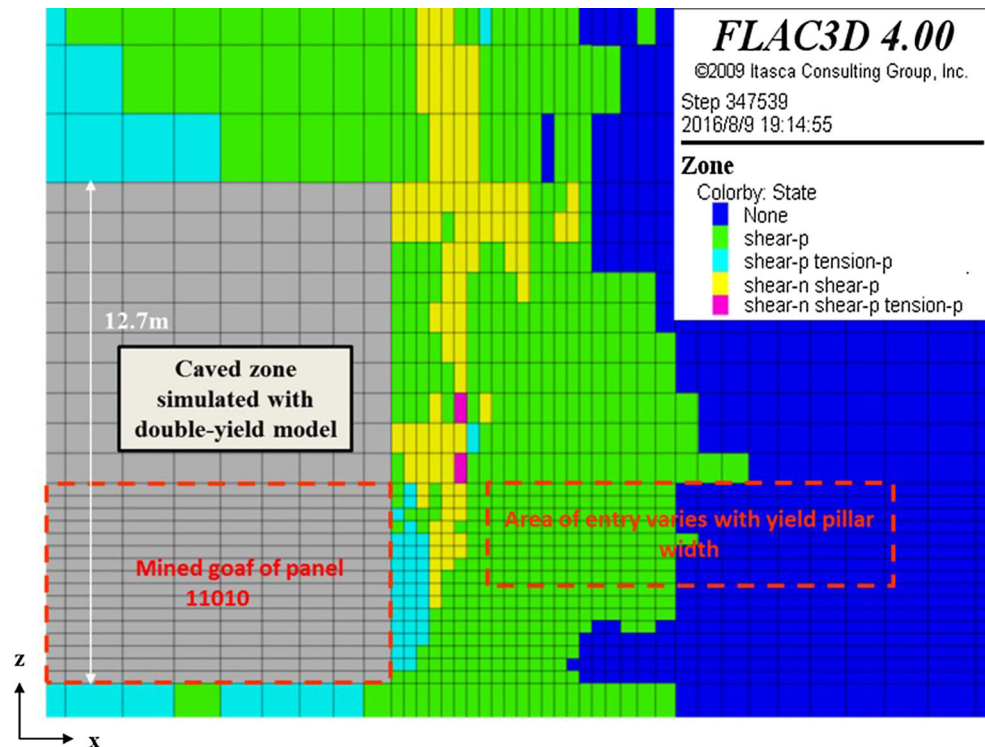Fig. 11 Global model for the EDG stability analysis. a Plan view of the model, b support design of the entry

Fig. 12 Vertical stress distribution after EDG development

Fig. 13 Failure zones induced by the extraction of panel 11,010 (cross-section)

EDG are strongly affected by the extraction of adjacent panels. As seen from Fig. 13, the coal extraction of panel 11,010 induces a large extent of failure zones, where the headentry of panel 11,030 will be excavated. Massive shear failure can be observed, but tensile failure only occurs near the exposed goaf surface. Under such circumstance, a significant difference in the total failure zone extent of the four models will not be observed, and it is generally difficult to determine the failure zones that are induced only by the entry excavation. Thus, the difference in ground failure with respect to different yield pillar widths is not described.

As demonstrated in previous studies (Shen 2014; Jiang et al. 2016), zones of tensile failure occur near the ground surface after entry development and can be used as an indicator for roadway stability analysis. Because no tensile failure is observed (from Fig. 13) at locations where the headentry with a different pillar width is about to be excavated, the extent of tensile failure after entry development should be a valid indicator for entry ground failure with respect to the different yield pillar widths. Therefore, zones of tensile failure within 2 m from the entry surface of four global models have been marked and are counted using FISH code. The distributions of tensile failure along one segment of the headentry are illustrated in Fig. 14. Note that the left side of the entry is the yield pillar and the right side of the entry is solid coal. Failure zone indicators that contribute to stability analysis are listed in Table 6.

Compared with the other three models from the results of Fig. 14 and Table 6, Model-3 m has the widest extent of tensile failure zones in the yield pillar and the most significant asymmetric failure between the left (pillar-rib) and right (seam-rib) sides of the entry. This occurs because the yield pillar with a 3 m in width not being wide enough to isolate the tensile failure zones of goaf (as shown in Fig. 13) from those newly propagated by the entry development, which results in the yield pillar undergoing severe tensile failure and instability. Because the entry is located farther from the goaf, the yield pillar is affected less by the mining activities of the goaf. Model-5 m has the least tensile failure zones in total and failure extent in pillar, but notably more tensile failure is detected in Model-3 m and Model-11 m. For Model-11 m, the large scale of tensile failure should be caused by the high stress state, as indicated in Sect. 4.2.

4.4 Evolution Characteristics of Ground Deformation During Entry Development

To comprehensively monitor the deformation evolution of the headentry during its service life, 10 monitoring points have been set at the monitoring station, as shown in Fig. 15. Deformation at monitoring points is recorded during their entire service life, which begins immediately after excavation and support installation and ends when the monitoring location is mined out and abandoned after the caving of the
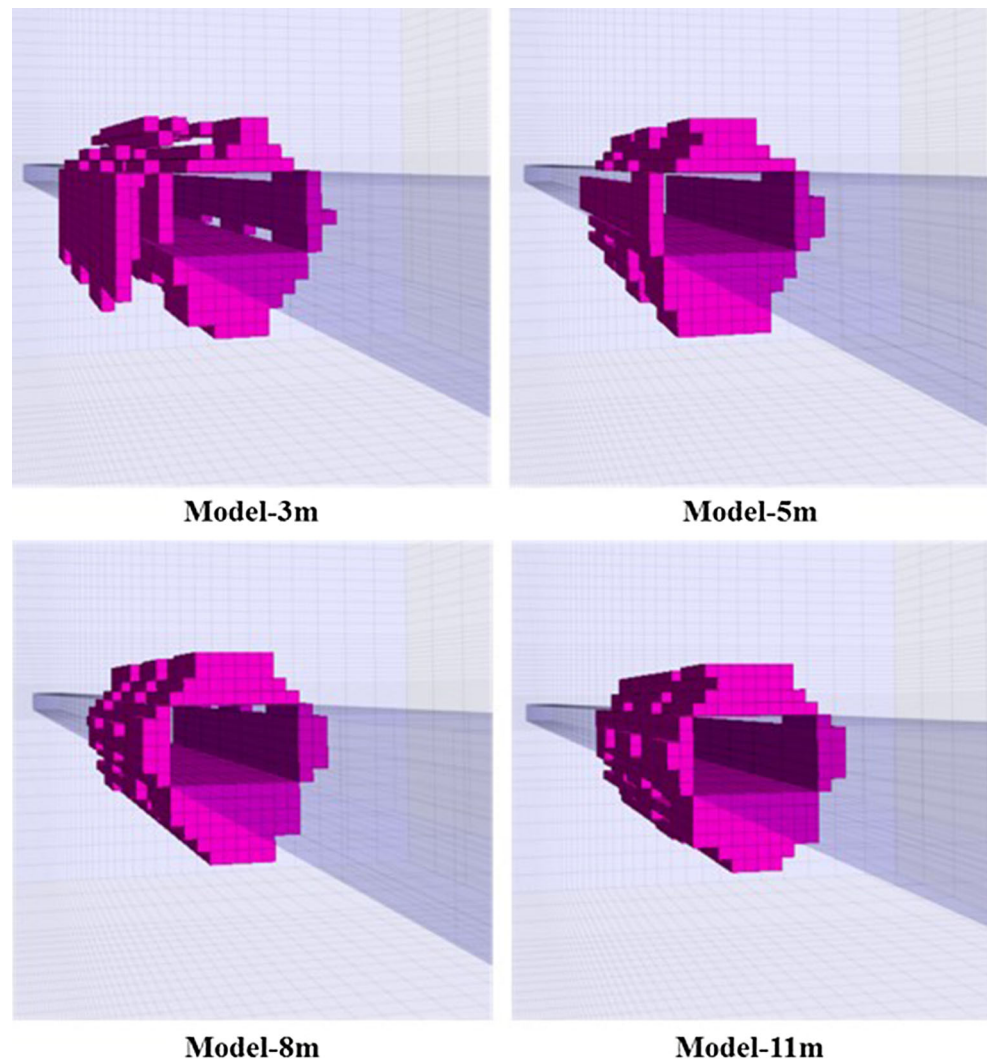
Fig. 14 Distributions of tensile failure zones

Model-3m

Model-5m

Model-8m

Model-11m

Table 6 Failure zone indicators for EDG stability analysis

Pillar width (m)	Number of zones within 2 m from entry surface	Number of tensile failure zones	Ratio of tensile failure (%)
3	11400	4742	41.6
5	11400	4050	35.5
8	11400	4552	39.9
11	11400	4899	43.0

roof. Such an arrangement aims to thoroughly monitor the ground deformation evolution induced by engineering disturbance (entry development and retreat mining).

Figures 16, 17 and 18 show the evolution of roof sag, rib convergence and floor heave for models with different yield pillar widths during the period of entry development.
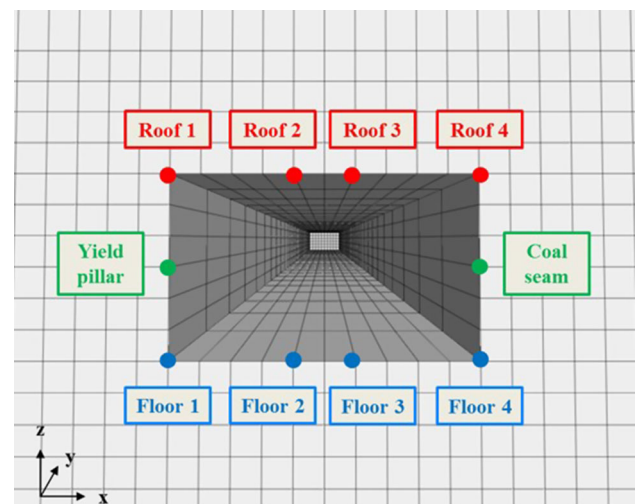
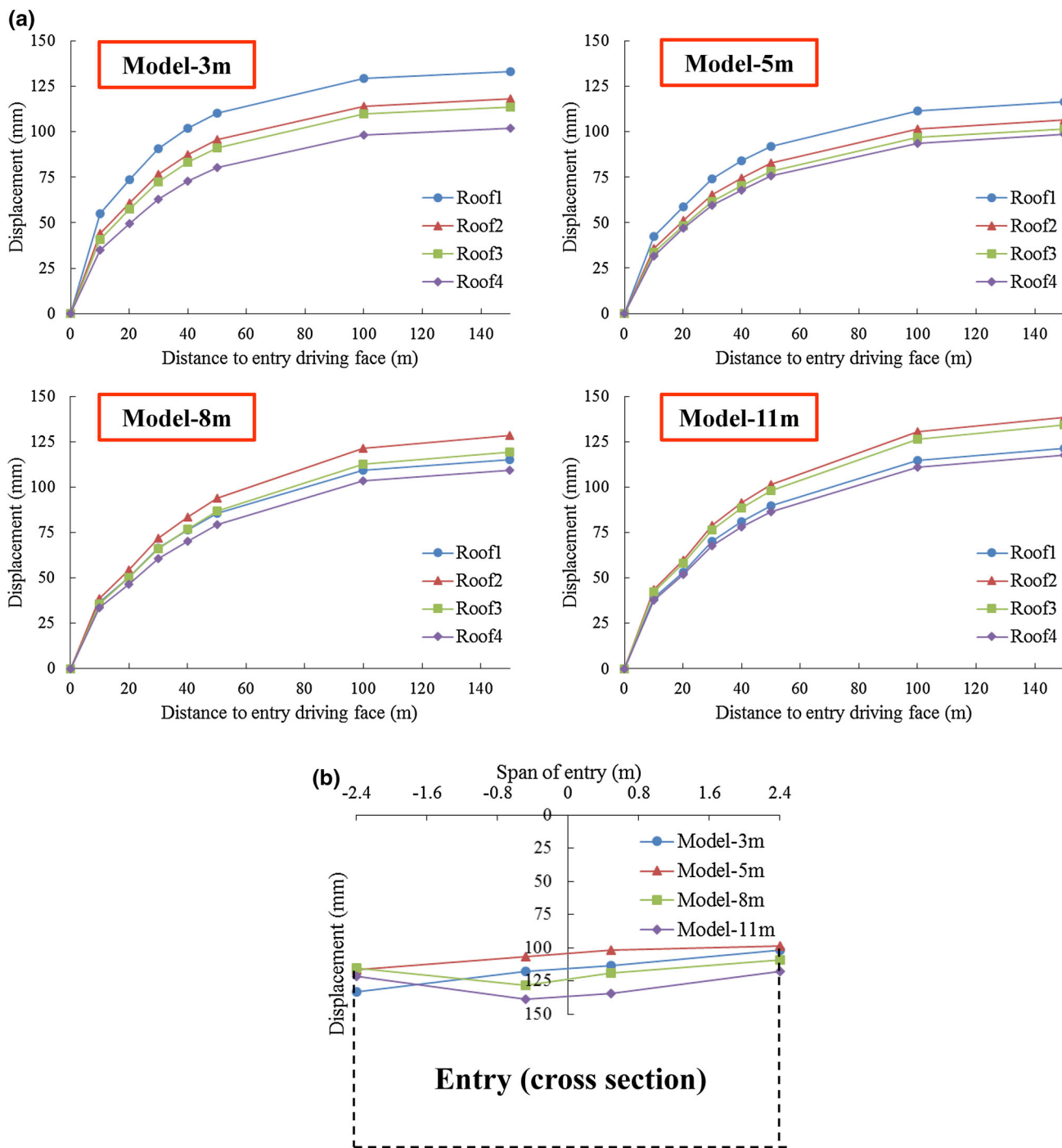**Fig. 15** Layout of monitoring points

Fig. 16 Roof sag during entry development with respect to different yield pillar widths. **a** Deformation evolution, **b** sketch of deformed roofline

It should be noted that the inward rib convergence shown in Fig. 17 is the sum of deformations of the two ribs. As seen, for all cases, large ground deformations occur right after the entry is driven, and the deformation increase rate gradually reduces with the progressive development of the entry.

Compared with the numerical study of a gateroad that is driven in solid coal in the same mine (Jiang et al. 2016), which has an identical strata layout, rock mass properties, constitutive models, and boundary conditions, a considerable creep deformation can be observed from ground deformations of EDG in the present study (Figs. 16, 17,
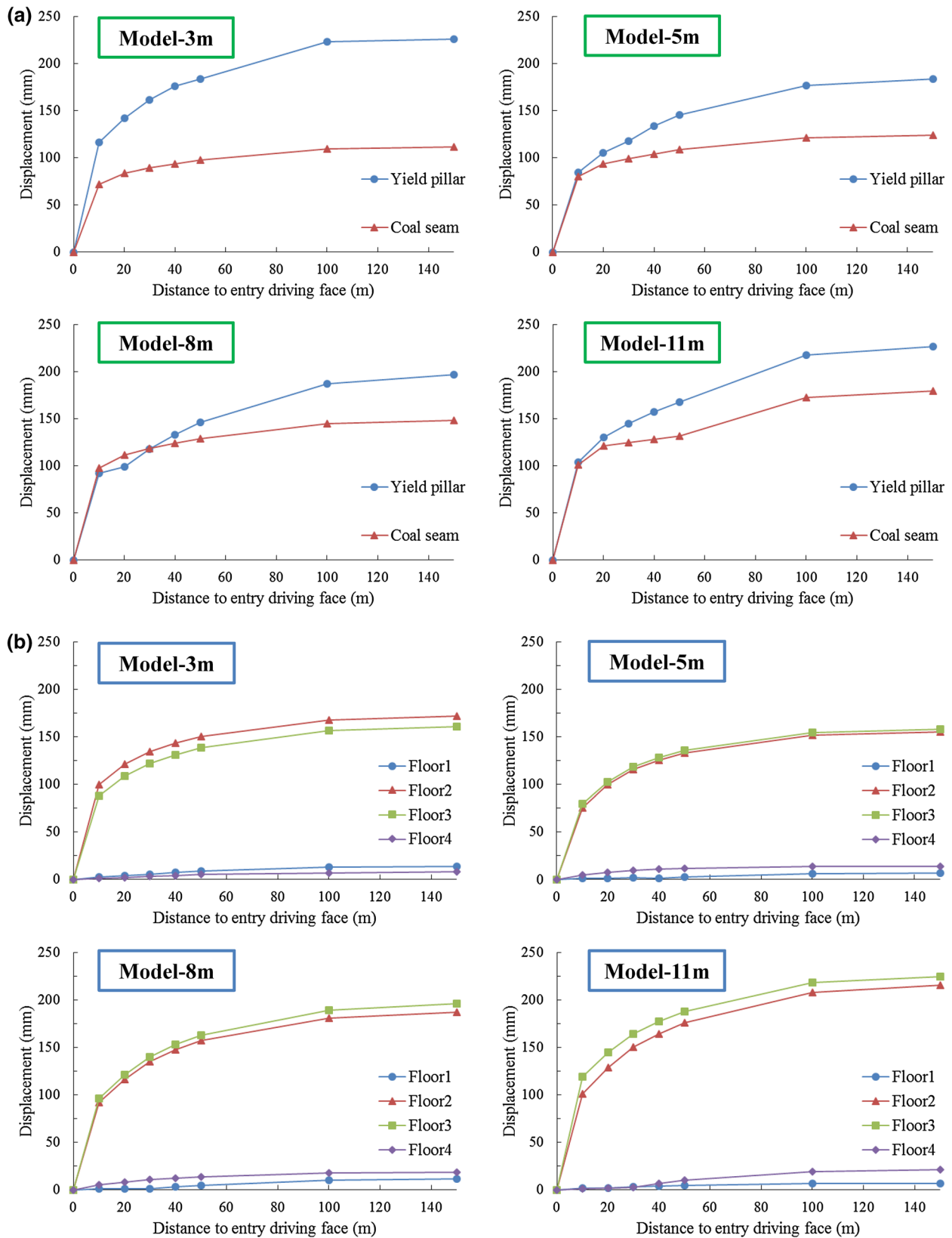
Fig. 17 Deformation of ribs and floor during entry development with respect to the different yield pillar width. **a** Rib convergence, **b** floor heave
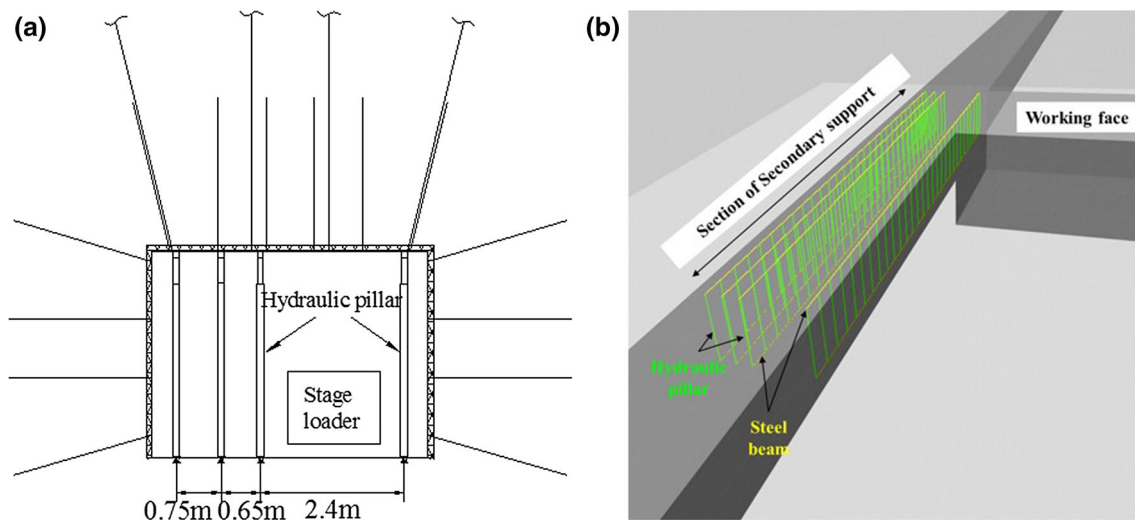
Fig. 18 Fore-support ahead of face (**a**) cross section of field support design, **b** numerical simulation

18). Taking Model-8 m as an example, 43.8% of roof sag, 32.0% of rib convergence and 28.0% of floor heave are generated after the driven face has advanced more than 30 m from the monitoring station. The observed creep ground behavior should be attributed to the yielded surrounding rock mass prior to entry development, which was caused by adjacent coal extraction, and it is one of the main ground characteristics of EDG in Chinese coalfields (Hou 2013).

The deformation patterns, which are recorded at multiple monitoring points, vary with the different yield pillar widths. In terms of roof sag, the displacement evolution at different locations of roof is shown in Fig. 16a. A sketch that exhibits the deformed roofline after entry development, obtained by comparing final displacements at four roof monitoring points, is illustrated in Fig. 16b. For Model-3 m and Model-5 m, most displacements occur on the left (pillar-side) corner of the roof, and a notable asymmetric deformation can be observed. The left corner has deformed significantly more than the right (seam-side) corner (31.3 mm for Model-3 m and 17.7 mm for Model-5 m). This characteristic weakens as the pillar width increases, which results from less yielded and fractured rock mass. When the pillar width increases to 8 and 11 m, the entry locates farther from the severely mining-affected zone, and the roof sag exhibits a general pattern with a maximum displacement occurring at the mid-span of the roof. However, a pillar with 8 or 11 m in width is not sufficient to fully isolate the mining influence from the adjacent panel. Some asymmetric deformations remain. That is, the left half-span (pillar-side) of roof has deformed more (9.4 mm for Model-8 m and 4.3 mm for Model-11 m) than the right half-span has (seam-side).

As seen in Fig. 17a, the convergence of both ribs is more significant than roof sag due to the weak properties of coal. Significant differences (114.5 mm for Model-3 m, 59.4 mm for Model-5 m, 48.3 mm for Model-8 m, and 42.0 mm for Model-11 m) between the convergence of pillar rib and seam rib should be noticed, consistent with field observation in Fig. 5. Due to the large span of the entry (4.8 m), a considerable difference in the stress and ground condition between the pillar rib and seam rib can be expected based on the aforementioned study. Coal in the pillar rib is more influenced by mining, which makes the stress and deformation release more than in the seam rib. The degree of asymmetric deformation reduces with an increase in pillar width due to the increase in distance from severely mining-affected coal and rock mass.

In case of floor heave, as presented in Fig. 17b, large displacements occur to the mid-span of floor, whereas the corners are deformed unnoticeably in all models. In contrast to the deformation pattern of roof and ribs, the floor heave does not present a noticeable asymmetric characteristic.

In terms of ground deformation during entry development, the simulation results of Model-8 m are in good agreement with the field monitoring presented in Sect. 2.3.

4.5 Evolution Characteristics of Ground Deformation During Retreat Mining

Because the mining process induces a series of intensive activities (Peng 2008), fore-supports with multiple rows of hydraulic pillars (model: DW35-200/100) are installed in the headentry and tailentry, with a range of 30 m ahead of the working face, as illustrated in Fig. 18a. The fore-support is simulated with structural elements, as illustrated in
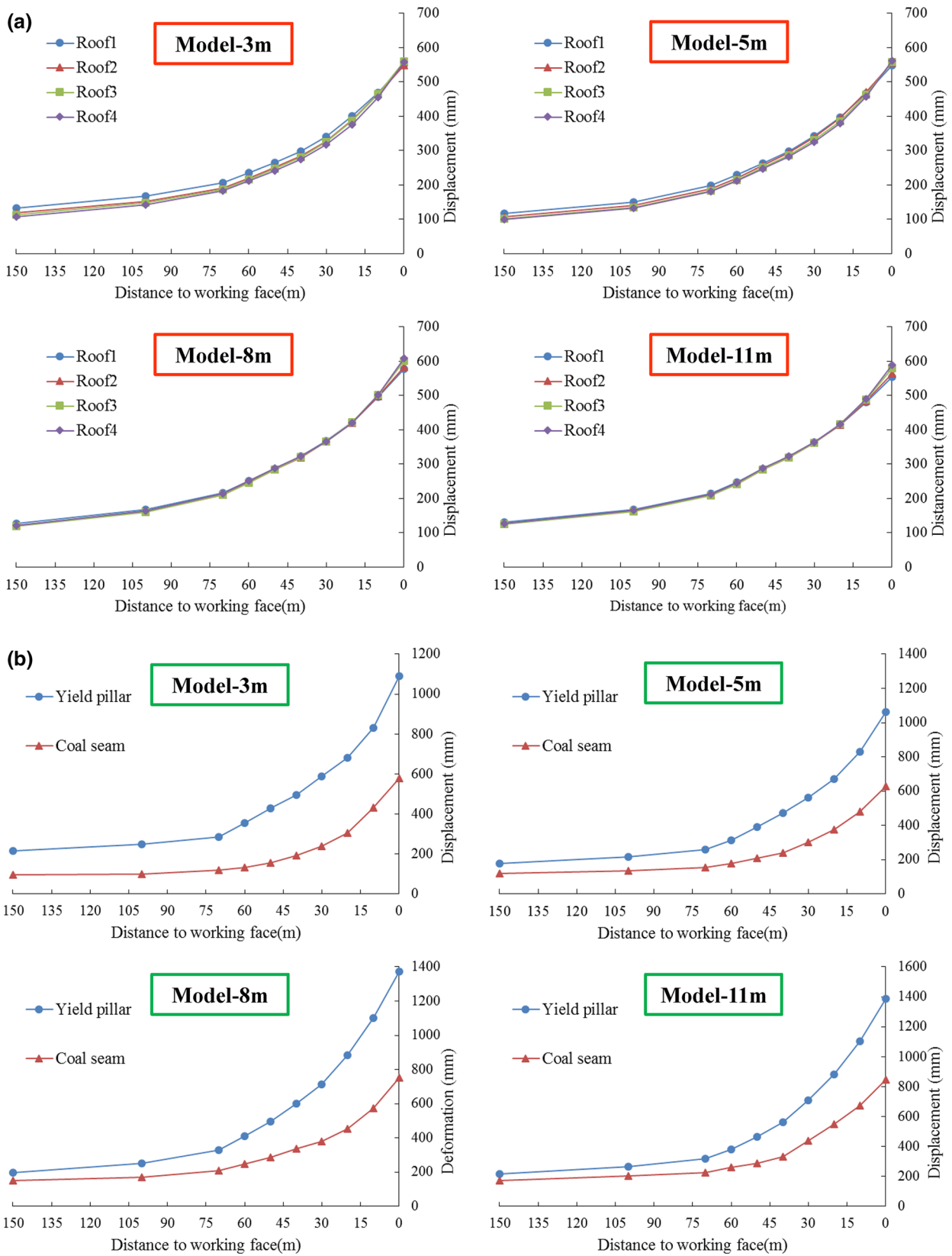
Fig. 19 Ground deformation during retreat mining with respect to different yield pillar widths. **a** Roof sag, **b** ribs convergence, **c** floor heave
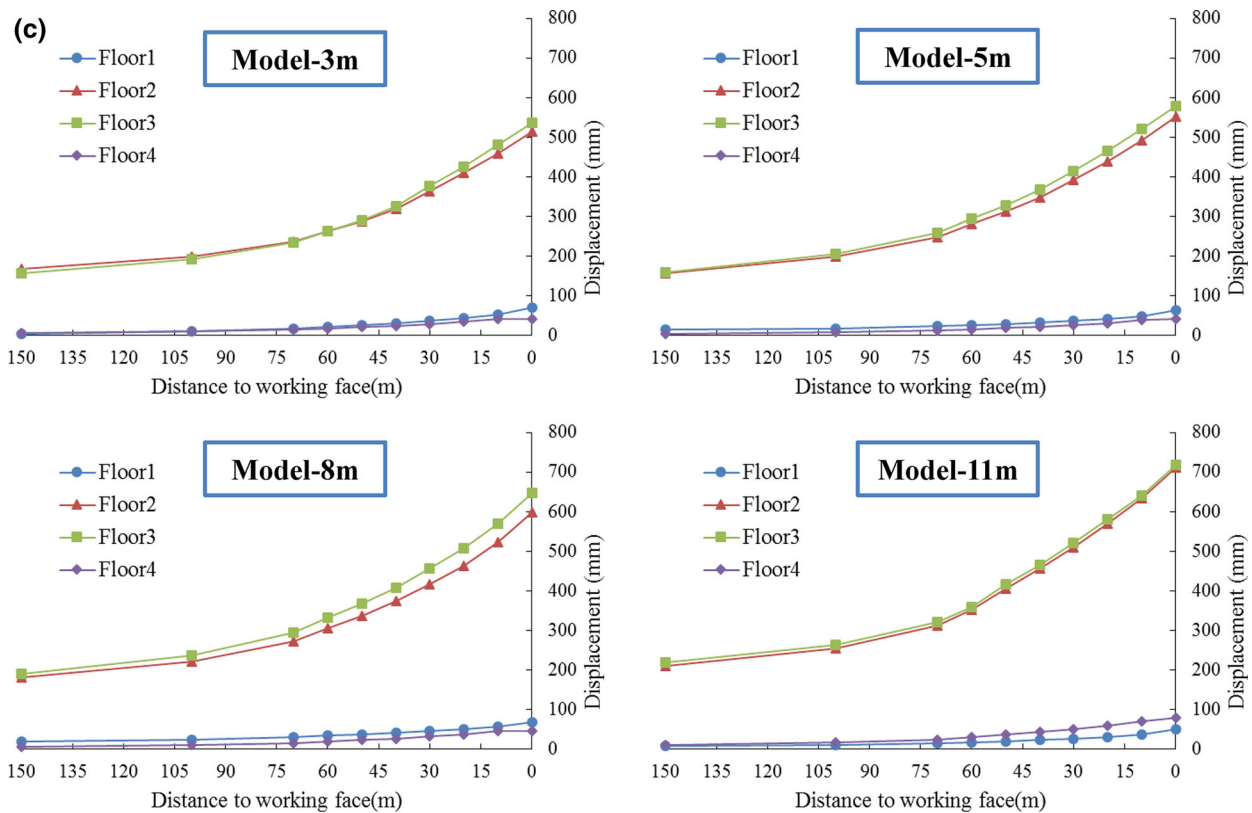
Fig. 19 continued

Fig. 18b, by employing the mechanical properties presented in Sect. 2.1.

Due to the intensive mining influence, massive ground failure around the entry is expected when the working face approaches, and the primary task is to prevent entry dysfunction that is caused by excessive deformation with a fore-support. Therefore, ground deformation evolution with the retreat of longwall face is the most valid indicator for stability analysis, as shown in Fig. 19. In all cases, the deformations increase moderately after the retreat mining begins, and the increasing rate is not noticeable until the working face reaches a distance of 70 m from the monitoring station. Then, the surrounding rocks of the entry begin to significantly deform until the monitoring station is mined out and abandoned. Due to the intensive and long-range mining influence, the entry undergoes significant ground destabilization and deformation, which requires a high-intensity fore-support to maintain its function.

Under the mining influence, the deformations of roof and floor present a generally symmetric feature (as shown in Fig. 19a, c), which can be attributed to the asymmetric high-intensity fore-support. However, due to the lack of effective fore-support, the asymmetric deformation between two ribs continues and grows with the approaching of working face, as shown in Fig. 19b. The deformation

difference reaches 513.4 mm (Model-3 m), 434.5 mm (Model-5 m), 621.6 mm (Model-8 m) and 542.8 mm (Model-11 m) by the end of entry service life. According to field practice, the mining-induced ribs convergence is so intense that the on-site operators have to terminate the displacement monitoring and repair the entry.

4.6 Effect of the Yield Pillar Width on Ground Deformation

As observed from Figs. 16, 17 and 19, the width of yield pillar has a considerable effect on ground deformation in the periods of entry development and retreat mining. Thus, vertical (roof-floor) and horizontal (two ribs) deformation at the end of each period is marked in Fig. 20 for comparison. During entry development, the correlation between pillar width and ground convergences is non-monotonic, and EDG with a 5-m-wide pillar has the least deformation under the current geological and geotechnical conditions. During retreat mining, convergence increases with the increase in pillar width, and the pillar width has more effect on rib convergence than roof-floor deformation.

As presented in Sects. 4.2 and 4.3, both stress and failure distribution within the surrounding rock after entry development have a positive correlation with pillar width
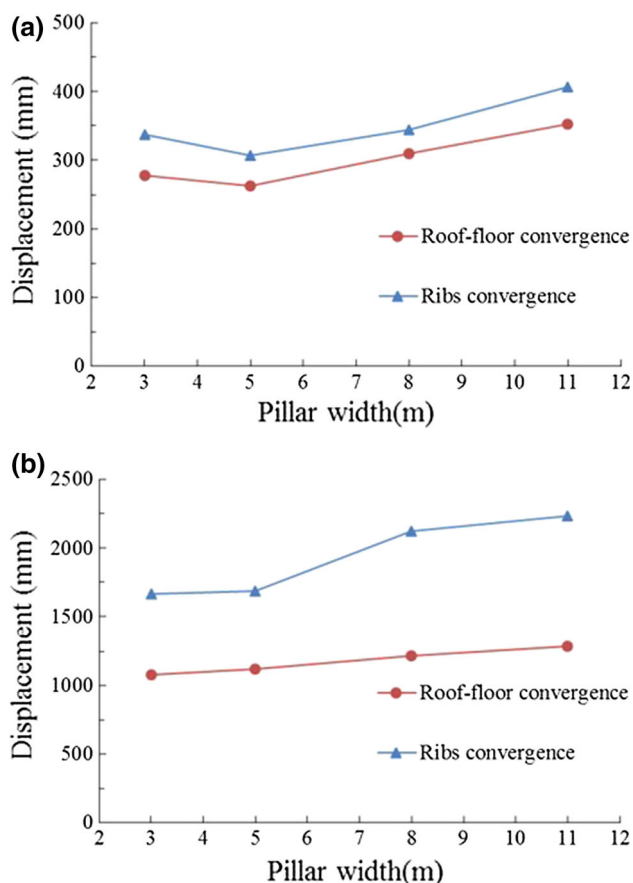
Fig. 20 Effect of yield pillar width on ground deformation. **a** Entry development period, **b** retreat mining period

when the width is wider than 5 m. When the entry undergoes a mining influence, the induced stress release and rock failure is more intensive, which ultimately results in greater ground deformation and instability. These results are consistent with the studies carried out by Bai (2006), Bai et al. (2004) and Yan et al. (2013), whose mechanism is explained by analyzing the mining-induced rotation and subsidence of key overlying strata (Hou 2013).

4.7 Discussion of Pillar Optimization of Panel 11,030

As presented above, the ground stability of different models was analyzed in light of stress distribution, failure extent and deformation evolution during the entire entry service life. Model-3 m has the least stress concentration after entry development and ground deformation after retreat mining, whereas Model-5 m has the least failure extent in surrounding rock and ground deformation after entry development. The models with wider pillars have worse ground stability in aspects of stress concentration, failure state of rock mass and deformation during service life. By employing methods of numerical simulation, field

practice and analytical modeling, Bai (2006) concluded that the optimal yield pillar width of EDG in Chinese coalfield is 4–5 m for soft coal seam and 3–4 m for medium hard coal seam, which agrees with the results of the presented study.

However, as stated in Sect. 1, the design of yield pillar in practice should consider multiple factors and effects. Because the headentry of panel 11,030 is the first EDG in the Zhaogu No.2 coal mine, a relatively conservative design that involves setting an 8-m-wide yield pillar was employed as a trial test and to prevent potential serious safety issues such as gas emission or water inflow from goaf 11,010. According to field monitoring, the trial test is effective in isolating gas and water, but the excessive ground deformation and instability have become the primary issues that incur massive costs for entry repair.

Based on the case study and numerical investigation presented in Sect. 4, a yield pillar with a width of 5 m may contribute to improving the resource recovery rate and ground stability and reducing the burst potential and economic loss due to repair or secondary support, while maintaining a good isolation effect.

5 Field Validation

Due to the geological variation and heterogeneity of field practice, it is extremely difficult to find two EDG sites with identical geological and geotechnical conditions for a field investigation of pillar width. To validate the employed numerical approach and suggested design, a field test has been carried out at the headentry of panel 11,070, a longwall panel adjacent to panel 11,050, as illustrated in Fig. 21a. The headentry of panel 11,070 starts to be excavated after panel 11,050 is mined out, and its first segment, with a length of 854 m, is driven with a 30-m-wide stiff pillar. Due to the severe ground instability issues that occurred in the trial EDG test of headentry 11,030 (Site 1), the mine decided to drive the second segment of headentry 11,070 (Site 2) along the goaf with a 6-m-wide yield pillar, and its support design is identical to that of Site 1. A deformation-monitoring program involving multiple monitoring stations has been set up, and the data from both monitoring stations are shown in Fig. 21b. Note that the monitoring is under entry development, during which no additional mining activities occurred. As seen from Fig. 21b, c, a notable creep behavior of surrounding rock can also be observed. Due to the variation in monitoring duration, instead of the recorded total deformation, the deformation rate is more comparable to that exhibited in the field test of Site 2. From these results, the deformation rates of both the roof-floor (2.2–3.0 mm/d) and rib convergence (4.8–4.9 mm/d) of Site 2 are consistently smaller

Fig. 21 Field validation
(**a**) plan view of the testing site,
b monitoring station T1043,
c monitoring station T1216
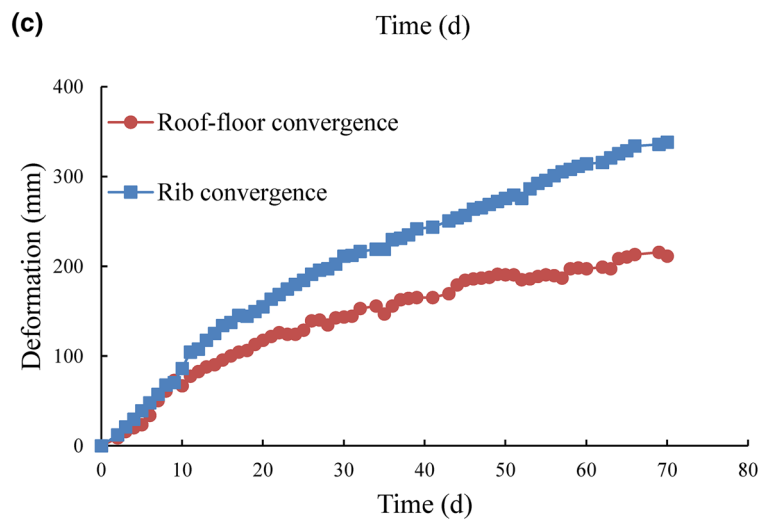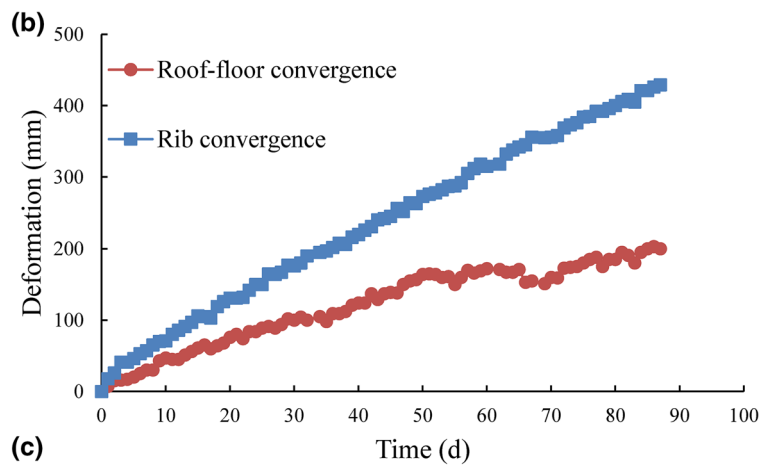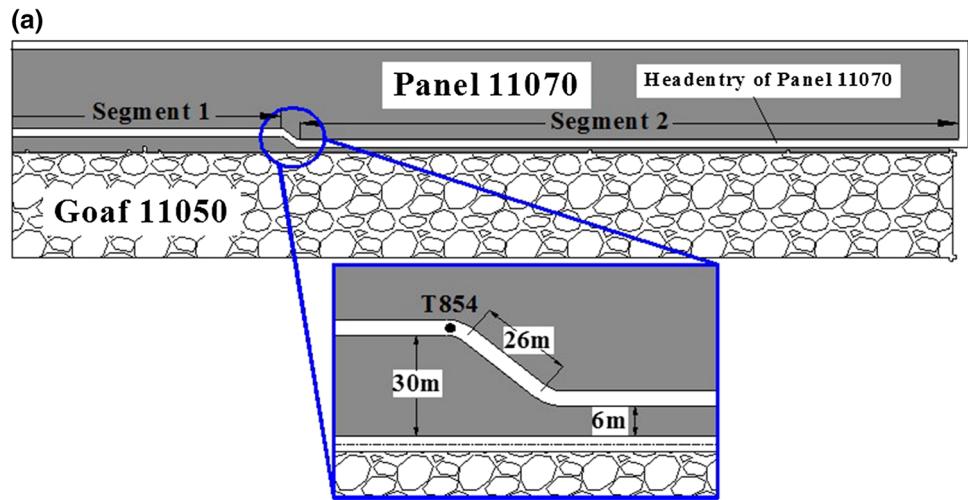
than those of the headentry of panel 11,030, as presented in Sect. 2.3 (4.0–10.1 mm/d for roof-floor convergence and 5.1–11.8 mm/d for rib convergence). In addition, the monitored gas concentration is 0.25%, and no water inflow has occurred. The results of this field test suggest that Site 2 manages to achieve better ground stability after yield

pillar optimization while maintaining the effectivity of isolating gas and water.

Although the geological variation may contribute to this deformation difference and the width of the yield pillar in Site 2 is 1 m wider than that in numerical study, the field test (Site 2) results indicate the success of ground control

by employing a yield pillar with an approximately 5–6 m width and serve to validate the numerical approach.

6 Conclusion

A case study on the trial test of EDG is carried out at the Zhaogu No.2 coal mine. According to the field observation and monitoring, the trial test shows good control for safety issues of gas or water by employing an 8-m-wide yield pillar, and excessive deformation and poor stability thus become the primary issues.

Based on the geological and geotechnical characteristics of EDG, the effect of yield pillar width on ground conditions and its design and optimization are comprehensively investigated via a numerical study, which considers the fracture-induced rock mass weakening and stress and ground condition that are affected by the mining activities of an adjacent panel.

Four global models with identical conditions, except for the width of yield pillar are built, and the effects that pillar width has on ground stability have been investigated by comparing aspects of stress distribution, failure propagation, and displacement evolution over the entire service life of the entry. According to the simulation results, vertical stress concentration around the entry shows positive correlation with the pillar width. Regarding the failure extent, Model-5 m has the least tensile failure zones in total and failure extent in the pillars. For ground deformation evolution during entry development, a considerable creep deformation can be observed. The notable asymmetric characteristics occur at the roof and ribs and tend to become moderate with an increase in pillar width. During entry development, the correlation between pillar width and ground convergence is non-monotonic, and EDG with a 5-m-wide pillar has the least deformation under the current geological and geotechnical conditions. During retreat mining, convergence increases with the increase in pillar width, and the pillar width has a greater effect on rib convergence than roof-floor deformation. The numerical study suggests that a 5-m-wide yield pillar may contribute to improving the resource recovery rate and ground stability and reducing the burst potential and economic loss due to repair or secondary support while maintaining good isolation effect. A field test carried out at an adjacent EDG contributes to validating the employed approach and suggested design.

By considering multiple mining-induced strata and rock mass responses, the present numerical approach instructs multiple analysis procedures as follows: (i) extent estimation of disturbed zones; (ii) back analysis of goaf properties with a double-yield model; (iii) estimation of a fracture-induced weakening parameter from field investigation; (iv) simulation and verification of a goaf-side stress environment; (v) mining operation simulation, including excavation sequence, progressive excavation, and rock support; and (vi) multi-parameter analysis. In addition, this study suggests an optimal EDG layout or yield pillar design by considering both ground stability and the isolation effect, which are acquired from numerical simulation and field practice, respectively. Validated by the field test, a new and comprehensive numerical approach is proposed. This approach makes progress in novel simulation techniques and procedures by analyzing multiple factors from both simulation results and field feedback. It serves to provide references and can be utilized for the evaluation, design and optimization of EDG and yield pillar under similar geological and geotechnical circumstances. This approach can be further improved by considering the periodic weighting of a roof.

References

Agapito JFT, Maleki HN, Moon M (1988) Two-entry longwall gateroad experience in a burst-prone mine. In: Proceeding of AMC international MINEXPO, vol II. American mining congress, Chicago, IL, pp 271–292

Bai JB (2006) Surrounding rock control of gob-side entry driving. China University of Mining and Technology Press, Xuzhou

Bai M, Kendorski FS, Van Roosendaal DJ (1995) Chinese and North American high-extraction underground coal mining strata behavior and water protection experience and guidelines. In: Proceedings of the 14th international conference on ground control in mining. West Virginia Univ., Morgantown, WV (United States), Proceedings of the 14th International Conference on Ground Control in Mining

Bai JB, Hou CJ, Huang HF (2004) Numerical simulation study of stability of narrow coal pillar of roadway driven along the goaf. Chin J Rock Mech Eng 20:3475–3479

Carr F, Martin E, Gardner BH (1984) How to eliminate roof and floor failures with yield pillar. Coal Min Part 1:62–70

Carr F, Martin E, Gardner BH (1985) How to eliminate roof and floor failures with yield pillar. Coal Min Part 2:44–49

Chen G (1989) Investigation into yield pillar behavior and design consideration. VPI and State University, PhD dissertation, pp 156

Chen JS, Peng SS (1999) Design of longwall face support by use of neural network models. Transactions Institute of Mining and Metallurgy Section A Mining Industry 108:A143–A152

Chen S, Wang H, Wang H, Guo W, Li X (2016) Strip coal pillar design based on estimated surface subsidence in Eastern China. Rock Mech Rock Eng 49:1–10

Hoek E, Carranza-Torres C, Corkum B (2002) Hoek-Brown failure criterion-2002 edition. Proceedings of NARMS-Tac 1:267–273

Hou CJ (2013) Ground control of roadways. China University of Mining & Technology Press, Xuzhou, China

Hou CJ, Ma NJ (1989) Stress in in-seam roadway sides and limit equilibrium zone. J China Coal Soc 14(4):21–29

Jiang LS, Liu HT, Lian XY, Zhang WW (2012) Research on rational width of coal-pillar in shallow-buried medium-thick coal-seam. Coal Min Technol 7(4):105–108

Jiang L, Sainoki A, Mitri HS, Ma N, Liu H, Hao Z (2016) Influence of fracture-induced weakening on coal mine gateroad stability. Int J Rock Mech Min 88:307–317

Li W, Bai J, Peng S, Wang X, Xu Y (2015) Numerical modeling for yield pillar design: a case study. Rock Mech Rock Eng 48:305–318

Morsy K (2003) Design consideration for longwall yield pillar stability. Dissertation, West Virginia University, pp 187

Peng SS (2008) Coal mine ground control, 3rd edn. Peng SS Publisher, Morgantown, WV, pp 229–237, 260-267, 422–423

Peperakis J (1958) Mountain bumps at the sunnyside mines. Min Eng 211:982–986

Salamon M (1990) Mechanism of caving in longwall coal mining. In: Rock mechanics contribution and challenges: proceedings of the 31st US symposium of rock mechanics, Golden, Colorado, Rock mechanics contribution and challenges: proceedings of the 31st US symposium of rock mechanics. Golden, Colorado, pp 161–168

Serata S (1982) Stress control method: quantitative approach to stabilizing mine openings in weak ground. In: Proceedings of the 1st international conference on stability in underground mining. Vancouver, BC, pp 52–93

Shen B (2014) Coal mine roadway stability in soft rock: a case study. Rock Mech Rock Eng 47:2225–2238

Tan YL, Yu FH, Ning JG, Zhao TB (2015) Design and construction of entry retaining wall along a gob side under hard roof stratum. Int J Rock Mech Min 77:115–121

Tsang P, Peng SS (1993) A new method for longwall pillar design. In: Proceedings of the 12th international conference on ground control in mining. Morgantown, WV, pp 261–273

Tu SH, Bai QS, Tu HS (2011) Pillar size determination and panel layout optimization for fully mechanized faces in shallow seams. J Min Saf Eng 28(4):505–510

Wang M, Bai JB, Li WF, Wang XY, Cao SG (2015) Failure mechanism and control of deep gob-side entry. Arab J Geosci 8(11):9117–9131

Wilson AH, Carr F (1982) A new approach to the design of multi-entry developments of retreat longwall mining. In: Proceedings of the 2nd international conference on ground control in mining. Morgantown, WV, pp 1–21

Yan S, Bai J, Wang X, Huo L (2013) An innovative approach for gateroad layout in highly gassy longwall top coal caving. Int J Rock Mech Min 59:33–41

Yavuz H (2004) An estimation method for cover pressure re-establishment distance and pressure distribution in the goaf of longwall coal mines. Int J Rock Mech Min 41:193–205

Zhang Z, Bai J, Chen Y, Yan S (2015) An innovative approach for gob-side entry retaining in highly gassy fully-mechanized longwall top-coal caving. Int J Rock Mech Min 80:1–11

Zhang GC, He FL, Jia HG, Lai YH (2017) Analysis of gateroad stability in relation to yield pillar size: a case study. Rock Mech Rock Eng 5:1–16

Zhao TB, Guo WY, Tan YL, Lu CP, Wang CW (2017) Case histories of rock bursts under complicated geological conditions. Bull Eng Geol Environ. doi:10.1007/s10064-017-1014-7